# We are IntechOpen, the world's leading publisher of Open Access books Built by scientists, for scientists

## 6,900
Open access books available

## 186,000
International authors and editors

## 200M
Downloads

Our authors are among the

## 154
Countries delivered to

## TOP 1%
most cited scientists

## 12.2%
Contributors from top 500 universities

**CLARIVATE ANALYTICS**

**BOOK CITATION INDEX**

**INDEXED**

**WEB OF SCIENCE**™

Selection of our books indexed in the Book Citation Index
in Web of Science™ Core Collection (BKCI)

## Interested in publishing with us?
## Contact book.department@intechopen.com

Numbers displayed above are based on latest data collected.
For more information visit www.intechopen.com

# Modified Metallic Oxides for Efficient Photocatalysis

Vladimir A. Escobar Barrios,
Dalia Verónica Sánchez Rodríguez,
Nancy Ayerim Cervantes Rincón and
Alma Berenice Jasso-Salcedo

Additional information is available at the end of the chapter

http://dx.doi.org/10.5772/intechopen.80834

### Abstract

The aim of the chapter is to present modified materials like alternatives for conventional photocatalyst such as titanium dioxide. Discussion about silver/graphene nanoparticles-modified zinc oxide for the degradation of pollutants like triclosan or bisphenol A, both considered as endocrine disruptors, which affect the hormonal development of humans, is presented. The best conditions to obtain the highest photodegradation degree are established. In addition, the bismuth oxychloride has gained attention during the last 5 years for photocatalysis. In accordance, the obtained results for phenol photodegradation, using such oxychloride, are also presented. In the chapter, the characterization of photocatalyst is reported along with the proposal for mechanisms of action for the modified ZnO photocatalyst and the bismuth oxychloride.

**Keywords:** ZnO, bismuth oxychloride, silver and graphene doped

## 1. Introduction

The photocatalysis has become an important research area in the recent years. The interest on such area has accelerated the number of papers, since photocatalysts have diverse applications, for example, the photodegradation of several contaminants that are quite difficult to transform to innocuous substance as water vapor. Other important applications are the development of self-cleaning products as well as the production of highly effective fuels like hydrogen. Nowadays, the technological development based on photocatalysis has an important growth in regions such as Europe and Asia (12% annually), with an estimated market of about € 1500 million in 2015 [1].

Photocatalysts are based on semiconductor materials, which are activated by radiation with higher energy than the bandgap of the used semiconductor, in order to create hole-electron pairs, once the electron passes from valence to conduction band. The promoted electron, toward conduction band, and the hole remained in valence band react in the photocatalyst interface with adsorbed substances in order to create reactive entities (free radicals and/or radical anions), which interact with contaminants to degrade them. All these processes imply the sorption on the photocatalyst's interface, its activation by radiation, creation of reactive species, and the recombination of electron to hole. The last could occur very fast that the creation of reactive species does not take place at great extent, giving ineffective photodegradation process.

In this context, the research regarding photocatalysis, in recent years, is focused to decrease the bandgap of photocatalyst in order to use solar light rather than UV light, which implies additional cost during the treatment process. In addition, minimization of the recombination process, in order to improve the photocatalytic performance, is quite important too. Some approaches to face these issues consider the doping with metals; meanwhile other research groups also consider the modifications with electron-rich species like graphene.

$TiO_2$ has been the photocatalyst by excellence and has been widely studied in its pristine form and/or doped with metals like gold and other elements. Nevertheless, other metal oxides, such as ZnO, have shown better photocatalytic performance, especially when visible light is used. ZnO has also been doped with metals like gold or silver. More recently, other metal oxides like bismuth oxychloride have gained attention for photocatalytic process.

In this chapter, discussion about the modification of ZnO with graphene is presented and discussed in terms of the implied mechanism (hybridization), in addition to the obtained results when such hybrid photocatalyst was used for the photodegradation of triclosan under visible light. Additionally, the modification method of ZnO with silver nanoparticles and its effect on photocatalytic performance for bisphenol A, Rhodamine B (RhB), and Triclosan is presented.

Finally, the use of an attractive photocatalyst, bismuth oxychloride (BiOCl), and its respective modification with silver and graphene oxide for RhB photodegradation along with the result and mechanism for the photocatalyst based on $TiO_2$-BiOCl used for photodegradation of phenol is presented and discussed.

The three different photocatalysts show how effective photocatalyst can be obtained and modified. The presented and discussed results contribute to understand some of the key parameters implied in the photocatalysis.

## 2. Zinc oxide

Zinc oxide (ZnO) is a II-VI group semiconductor with wurtzite structure with lattice parameters a = 0.3296 nm and c = 0.52065 nm. $Zn^{2+}$ atoms are tetrahedrally coordinated with $O^{2-}$ atoms stacked alternately along the $c$ axis so that d-electrons of zinc are hybridized with 2p-electrons of oxygen [2]. ZnO has the potential to become an important material for photocatalysis because it is nontoxic (it is often included in pharmaceuticals), photostable, and low cost.

We consider at least three windows of opportunity to boost ZnO as photocatalyst in academy and industry. The first is related to the quantum yield in visible light rather than UV for the efficient utilization of the electron-hole ($e^-/h^+$) pairs during decomposition of endocrine disruptors and emergent contaminants in water. A second opportunity is the immobilization of the photocatalyst that could make possible its utilization on continuous mode and toward implementation at industrial scale. The third challenge deals with nonlinear mathematical modeling of the factors that rule the photocatalytic kinetics of the metallic-modified ZnO for optimization purposes. This is not a trivial problem in photocatalysis and artificial neural network tools (ANNs) do not demand of academic expertise for a fast implementation; for example, in the industry sector. The reader can consult [3] for the approach that Meimaroglou and collaborators follow to assess ZnO photocatalyst structure-photocatalytic performance associations toward the maximization of the photocatalytic efficiency. The first two challenges are addressed in the present chapter.

## 2.1. Use of ZnO/graphene photocatalysts

Nowadays, solar energy, radiant light, and heat from the sun are the most abundant available sources of clean energy. Thus, research studies and development of materials that can efficiently harvest solar irradiation and used for green environmental pollution management are essential. Photocatalysis, which could use renewable solar energy to activate the chemical reactions via oxidation and reduction, such as that occurs in advance oxidation processes (AOPs), is a sustainable technology to provide solution for environmental issue. This photocatalysis system has attracted great interest from science community as the most promising way to solve the environmental problems, especially getting rid of residual pollutants from wastewater stream.

In the field of photocatalysis, ZnO has emerged as the leading candidate for green environmental management systems because of its unique characteristics, such as wide bandgap (3.37 eV) in the near-UV spectral region, a large electron exciton binding energy of 60 eV at room temperature, strong oxidation ability, and good photocatalytic property [4]. It is a well-known fact that ZnO occurs as white hexagonal crystal or white powder known as white zinc. ZnO crystallizes in the wurtzite structure and is available as large bulk single crystals [5]. As an important semiconductor material, ZnO has been applied in catalysis, rubber and paint industries, ceramic bodies, varistors, fertilizers, and cosmetics [6].

Recently, the development of ZnO with precisely controllable features has gained significant scientific interest. The electrical, optical, and magnetic properties of ZnO can be altered or improved by the use of ZnO in nanoscale and efforts have been developed to improve the properties of ZnO photocatalyst [7]. Moreover, ZnO is an environmental friendly material as it is compatible with living organisms [8]. Since ZnO has almost the same bandgap energy as $TiO_2$ (3.2 eV), its photocatalytic capability is anticipated to be similar to that of $TiO_2$. However, ZnO is relatively cheaper compared to $TiO_2$, whereby the usage of titanium dioxide is uneconomic for large-scale water treatment operations [9]. The greatest advantage of ZnO is the ability to absorb a wide range of solar spectrum and more light quanta than some semiconducting metal oxides including the capacity to absorb visible light energy, which is due to its

wide band energy. This results in fast recombination of photogenerated charges and thus caused low photocatalytic efficiency.

The recombination of photogenerated hole ($hVB^+$) and electron ($eCB^-$) is one of the major disadvantages in semiconductor photocatalysis. This recombination step lowers the quantum yield and causes energy wasting. Therefore, the $e^-/h^+$ recombination process should be inhibited to ensure efficient photocatalysis. Metal doping could counter the recombination problem with efficient charge separation between electrons and holes in ZnO photocatalyst. In addition, the dopants may trap electrons, reducing the chances of $e^-/h^+$ recombination that deactivate the photocatalytic system [10]. Furthermore, the generation of hydroxyl radicals and active oxygen species will greatly increase resulting from the enhancement in charge separation efficiency [11]. Semiconductors as graphene have been proven as a couple semiconductor that can improve the visible-light photocatalytic efficiency of ZnO due to its remarkable chemical, physical, and mechanical properties, such as large surface area (2600 $m^2$/g), excellent electrical and thermal conductivity, high mechanical strength, flexibility, and efficient wide range of light adsorption. Due to the properties of graphene-based materials, several ranges of environmental applications have been developed such as absorption, transformation, and detection [12]. So far, numerous methods have been used to design and synthesize ZnO/graphene hybrid photocatalysts with various morphologies. However, most of these methods rely on chemical and/or high-energy consumption resulting in a costly, environmentally hazardous, and especially inefficient photocatalyst for complete degradation of organic pollutants as triclosan, which has been classified as potential endocrine disrupting compound (EDC). Triclosan was ranked as the most abundant compound among all investigated pharmaceuticals and personal care products with its mean concentration of 12.6 $\pm$ 3.8 mg/Kg in 110 biosolids samples collected from 94 US wastewater treatment plants across 32 states and the District of Columbia using EPA Method 1694 [13]. In addition, the highest initial concentrations of triclosan detected in municipal biosolids were 2715 and 1265 µg/Kg [14].

Hydrothermal and chemical reductions have been the main methods studied to obtain ZnO/graphene hybrid photocatalysts. However, photodeposition method [15] has been reported as an efficient method to generate hybrid photocatalyst to degrade pollutants. This study proposes the synthesis of ZnO/graphene semiconductors by developing a facile, cheap, environmentally and high reproducibility approach to obtain an efficient material to degrade organic pollutants, as triclosan (TCS), under visible light. For instance, it has been demonstrated that inductive irradiation method is possible to synthesize ZnO composites due to its polarity [16]. In particular, graphene has the ability to accept electrons efficiently due to the absence of oxygen chemical groups on its surface preventing the recombination and providing a favorable π-π conjugation between TCS and aromatic region of graphene (**Figure 1**). The trapped electrons on graphene react with the dissolved oxygen and water to form reactive superoxide and hydroxyl radicals, which further oxidizes triclosan.

The modified photodeposition method has resulted in a successful process to prepare ZnO/graphene hybrid photocatalysts with enhanced photocatalytic activity under visible light radiation. The obtained results show degradation of 1% of triclosan (8 ppm) in absence of catalyst (photolysis) while this degradation percentage increases up to 42% using 0.5 wt% of
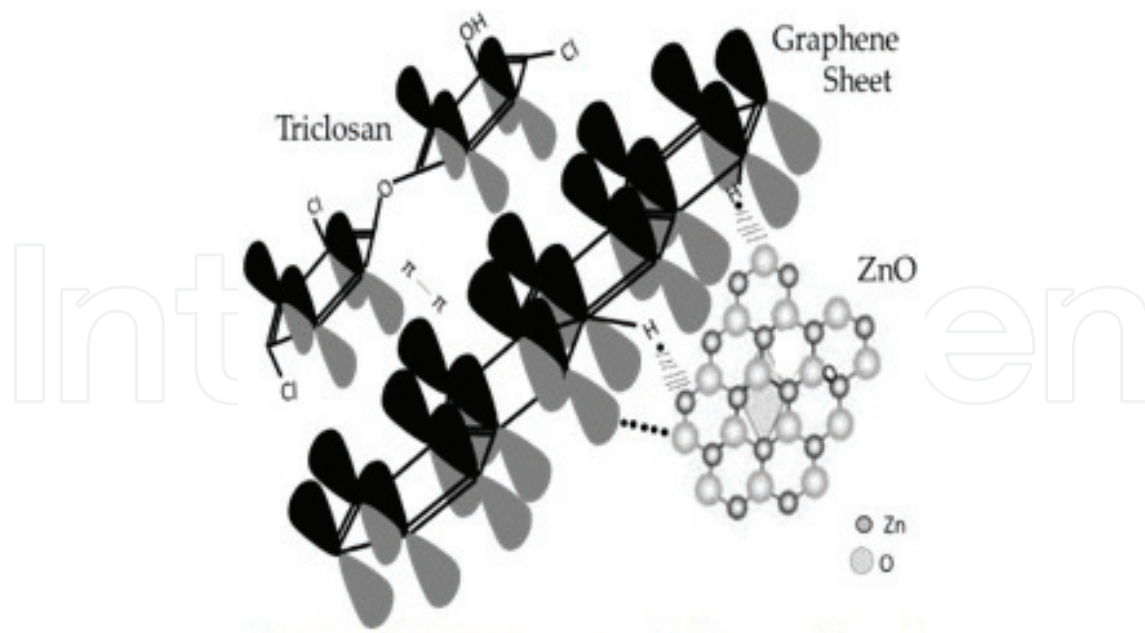
**Figure 1.** Schematic illustration of the interaction between ZnO photocatalyst doped with graphene sheets and its interaction with triclosan.

graphene sheets as dopant in ZnO nanocatalyst. It is important to mention that wurtzite has been the structure used in this study with a bandgap of 3.21 eV obtained by UV-vis spectrophotometer, while a value of 3.15 eV for ZnO/graphene composite was obtained. This reduction in the bandgap value is associated to a structure based on good interaction between ZnO nanocatalyst and graphene sheets, which creates intermediate energy levels between both materials, a property that allows to transfer the electrons promoted from the valence band to the conductive band of the ZnO semiconductor to graphene sheets that capture and retain the transferred electrons, improving the photocatalytic performance of ZnO as it is illustrated in **Figure 2**. This important first approximation has been the result of the evaluation of the effect of the loaded graphene amount in zinc oxide nano-photocatalyst. Graphene concentrations of 0.25 and 0.5 wt% were evaluated for this purpose and the obtained results showed enhancement of the ZnO photocatalytic activity under visible light radiation even using minimum contents of graphene sheets. Thus, 34 and 36% of the initial concentration of triclosan (8 ppm) was degraded using ZnO/graphene composites loaded with 0.25 and 0.5 wt% of graphene, respectively, and the bandgap values were 3.19 and 3.18 eV, for such ZnO/graphene composites. In contrast with 25% of initial triclosan degraded using pristine ZnO (bandgap: 3.21 eV). These results can be compared with those reported in previous investigations related with the photodegradation of triclosan using dopants such as rare-earth elements as Ce (47%) [17], metals such as Au (10% after 5 h) [18], Ag [19], and Cu [20]; as well as oxide compounds as MgO, WO$_3$, TiO$_2$, ZnO, or graphene oxide [21] using dopant contents up to 10%.

The adsorption properties of the as-prepare ZnO/graphene hybrid photocatalysts doped with different amounts of graphene sheets were one of the most important characteristics to improve the degradation efficiency of the ZnO. The specific area of ZnO and ZnO/graphene

hybrid photocatalysts was determined via $N_2$ adsorption isotherms using the Brunauer Emmett Teller (BET) method. The results revealed that the graphene monolayers (44.2 g/m$^2$) showed the highest surface area for the analyzed pristine material, while ZnO had a specific area of 10.8 g/m$^2$. Among the three investigated composites, the photocatalyst loaded with 0.5 wt% of graphene had the highest surface area (18.3 g/m$^2$), followed by ZnO/graphene 0.25 wt% (14 g/m$^2$) and ZnO/graphene 0.1 wt% (13.3 g/m$^2$) catalysts. Thus, the addition of graphene sheets increases the surface area of the hybrid catalysts up to 69% of the initial area of zinc oxide and improve their adsorption capacities, resulting in the first property of the as-prepare hybrid composites to increase the degradation of triclosan, as it has been reported previously [22].

In order to study the effect of the method of synthesis in the ZnO/graphene hybrids, composites were prepared by impregnation method with graphene contents of 0.5 wt% using continuous stirring in the absence of UV radiation. The resultant photocatalysts were tested to degrade triclosan under visible light radiation, and it was obtained that 15% of the initial concentration of triclosan was degraded, 53% less than the composites synthesized by photodeposition method as it can be observed in **Figure 2**.

The hybridization of ZnO with graphene has been studied and confirmed by Raman spectroscopy integrating the intensity ratio of the D to G bands characteristic for carbon materials. The G peak arises from the stretching of C-C bond of graphite materials and is highly sensitive to strain effects in sp$^2$ system, while D peak is caused by the disordered structure of graphene material. Regarding the sp$^3$ and sp$^2$ hybridizations $I_D/I_G$ value, in the case of pristine graphene oxide was 0.93, indicating that the intensity of the G band is higher than D band, which results in a lower amount of sp$^3$ defects and less structural disorder. Compared with graphene oxide (0.93), the reduction of $I_D/I_G$ ratio for ZnO/GO 0.5 wt% hybrid photocatalyst ($I_D/I_G$ = 0.91) is observed, implying a reduction of sp$^3$ defects compared with pure graphene oxide. This fact
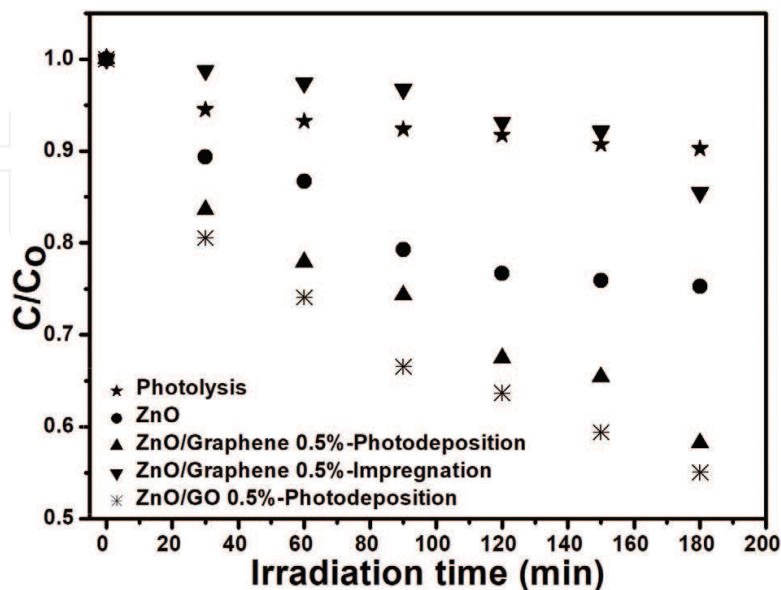


**Figure 2.** Degradation curves of triclosan under visible light radiation conditions: 23°C, pH = 7.

confirms the interaction between ZnO and GO given by $sp^3$ defects. The results given herein-above are consistent with the results in FTIR characterization, revealing the reestablishment of the conjugated graphene oxide network. In contrast, the ratio $I_D/I_G$ for the composite prepared with graphene sheets was calculated and corresponds to the value of 1.04 (higher than $I_D/I_G$ of pristine graphene, 0.36) indicating the presence of more defects in the graphene oxide lattice, which implies a decrease in the size of the in-plane $sp^2$ domains and formation of the defects and disorders in the graphene sheets, revealing the reestablishment of the conjugated graphene network ($sp^2$ carbon) [23] in the ZnO/GO photocatalysts due to the hybridization of graphene via photoirradiation method but resulting in a weak interaction due to the absence of chemical groups on the surface of graphene sheets as are presented on GO surface. The interaction between graphene oxide sheets was improved by the interaction of ZnO-polarized structure and the chemical surface of graphene oxide, which contains carbonyl, carboxyl, epoxy, and hydroxyl groups.

The degradation curves of triclosan for ZnO/GO hybrid photocatalyst are presented in **Figure 3**. It is noticed that the composites obtained by the photodeposition method are the materials with the best performance to degrade triclosan under visible light radiation compared with photolysis experiment and with the degradation using the bare ZnO photocatalyst.

In addition to the photodegradation curves presented in **Figure 3**, the rate constants are presented in **Table 1**.

The results show the highest apparent degradation rate constant for the hybrid catalyst synthesized with graphene oxide (0.003 $\text{min}^{-1}$), almost four times higher than the pristine ZnO semiconductor, corroborating the importance of interaction between ZnO and GO.



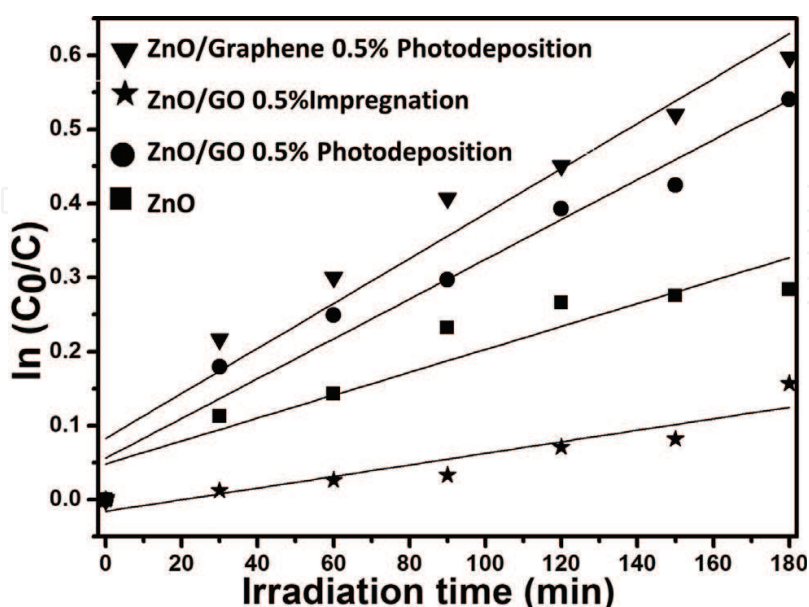**Figure 3.** Triclosan photodegradation curves with ZnO/graphene and ZnO/GO hybrid photocatalysts under visible light. Conditions: 23°C, pH = 7.

| Photocatalyst | $K_{appr}$ min$^{-1}$ |
|---|---|
| ZnO | 0.00078 |
| ZnO/G $_{PD}$ | 0.0016 |
| ZnO/ OG $_{IMP}$ | 0.0027 |
| ZnO/ OG $_{PD}$ | 0.003 |

**Table 1.** Apparent rate constants for triclosan photodegradation under visible light.
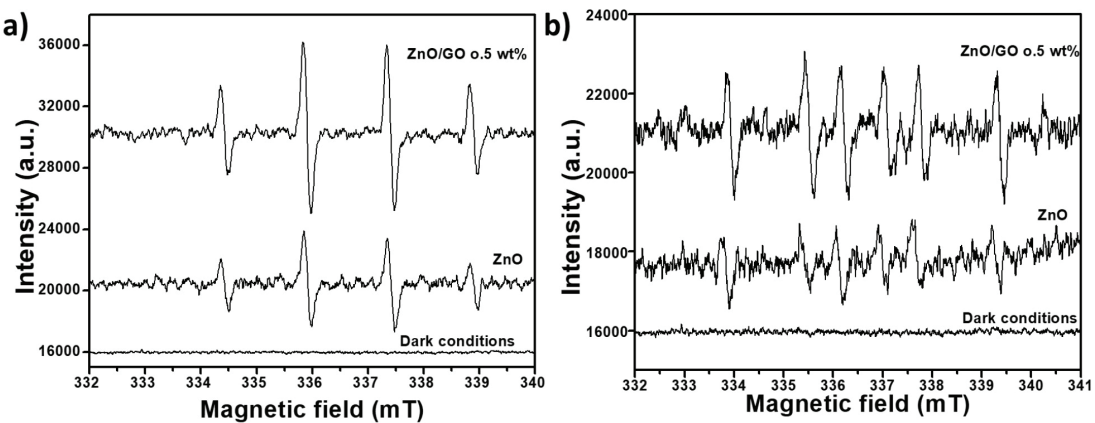


**Figure 4.** EPR spectra of ZnO/GO hybrid photocatalyst irradiated under visible light in (a) water and (b) ethanol solvents. DMPO was used as a radical trapper.

The mechanism of the best as-prepare ZnO/GO hybrid composite was proposed. Thus, the ESR spin-trap technique (with DMPO) was used to monitor the reactive oxygen species generated during the irradiation of the hybrid photocatalyst and the results are shown in **Figure 4**. Both signals of DMPO-$^\bullet$OH and DMPO-O$_2$$^{\bullet-}$ are clearly observed when pristine ZnO and ZnO/GO were exposed to visible radiation. Therefore, a dual mechanism involving both hydroxyl radicals and superoxide radicals is expected in the photocatalytic process. However, the signals for hybrid photocatalysts are stronger than the signals in pristine ZnO, thus accounting for the higher and stable photocatalytic performance of hybrid composites than bare ZnO toward the degradation of triclosan. The hydroxyl radicals trapped by DMPO (DMPO-$^\bullet$OH) and superoxide radicals (DMPO-O$_2$$^{\bullet-}$) for ZnO and hybrid photocatalysts were characterized by detecting four characteristic signals in water, and six signals in ethanol for DMPO-$^\bullet$OH and DMPO-O$_2$$^{\bullet-}$, respectively. In both cases, it is noticed that the signals for hybrid material are more pronounced than those for the ZnO pristine sample, thus accounting for the better photocatalytic performance.

Thus, the enhanced photocatalytic activity of ZnO/GO photocatalyst is due to the introduction of carbon material, which promotes an increase in charge separation to effective utilization of electrons to produce more $^\bullet$OH and O$_2$$^{\bullet-}$ radicals. In this case, the signals of $^\bullet$OH radicals are

stronger than those for $O_2^{\bullet-}$, which suggests the predominance of oxidative reactions whose holes are responsible for the degradation of triclosan. Furthermore, ZnO photocatalyst presents visible light photocatalytic activity but generates stronger visible light after graphene hybridization, showing that graphene oxide is responsible for the visible light performance, which is induced by the injection of an excited electron from the lowest unoccupied molecular orbit (LUMO) of graphene to the conduction band (CB) of ZnO. The introduction of the graphene semiconductors can possibly cause the rapid separation of electron-hole pairs during irradiation [11] prolonging the electron-hole pair lifetime and accelerating the transfer rate of electrons [24] as shown in **Figure 5**.

In conclusion, the adsorption properties, good interaction between ZnO- and graphene-based materials, chemical structure of graphene, method of synthesis, and concentration of the dopant used to hybridize ZnO catalyst are the most important properties that affect the development of ZnO/graphene hybrid photocatalysts.

## 2.2. ZnO modification by inorganic molecules: silver

Silver nanoparticles are linked to the ZnO surface through the alkanethiol surfactant (**Figure 6a**). The stabilizer ligands $COOH-(CH_2)_n-S-Ag$ keep nanoparticles as small as 7 nm in the solution and 15–26 nm in the Ag/ZnO photocatalyst, corroborated by XRD; although TEM analysis shows Ag nanoparticles of spherical shape and defined boundaries smallest as 3 nm over ZnO surface (**Figure 6b-d**). We studied the effect of the pH and time on the functionalization of ZnO nanoagglomerates by two methods denominated as photodeposition (PD) and impregnation (IMP) [15]. We propose to replace the ambiguous terms "doping" with functionalization when spoke of superficial ZnO modification. For instance, the sample 1%Ag/ZnO-PD11,1 synthesized by the PD method using 1 wt.% Ag at pH 11 and 1 h under UV light, a functionalization yield of 100% was corroborated by elemental analysis by inductively coupled plasma spectrometry ICP-OES and SEM-EDX. The UV irradiation produces free radicals ($^{\bullet}OH$, $^{-\bullet}O$) that degrade the ligand and release the silver nanoparticles onto the ZnO surface (**Figure 6c**). Byproducts of surfactant decomposition accumulate in ZnO are observed by IR. This functionalization of the
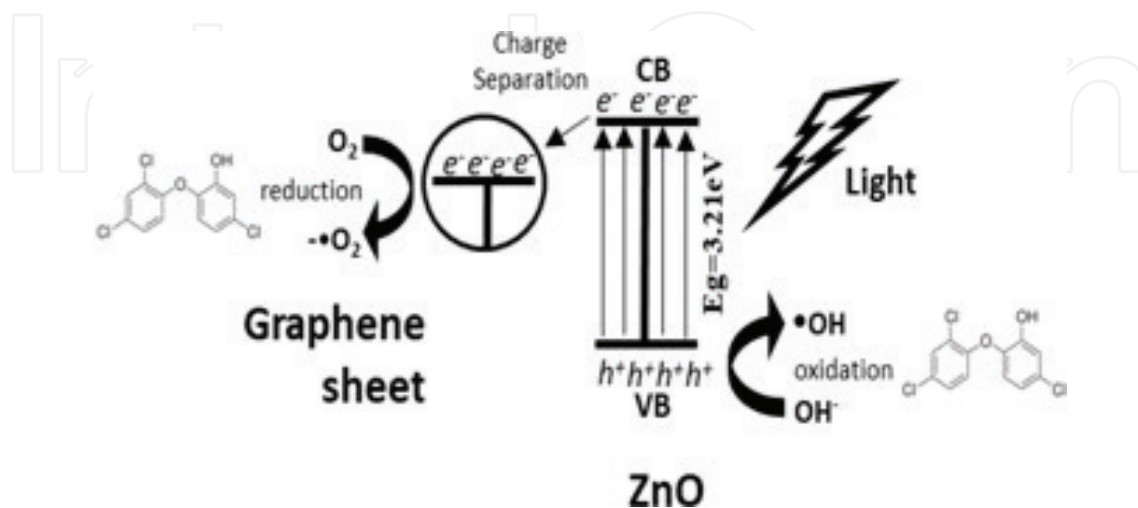


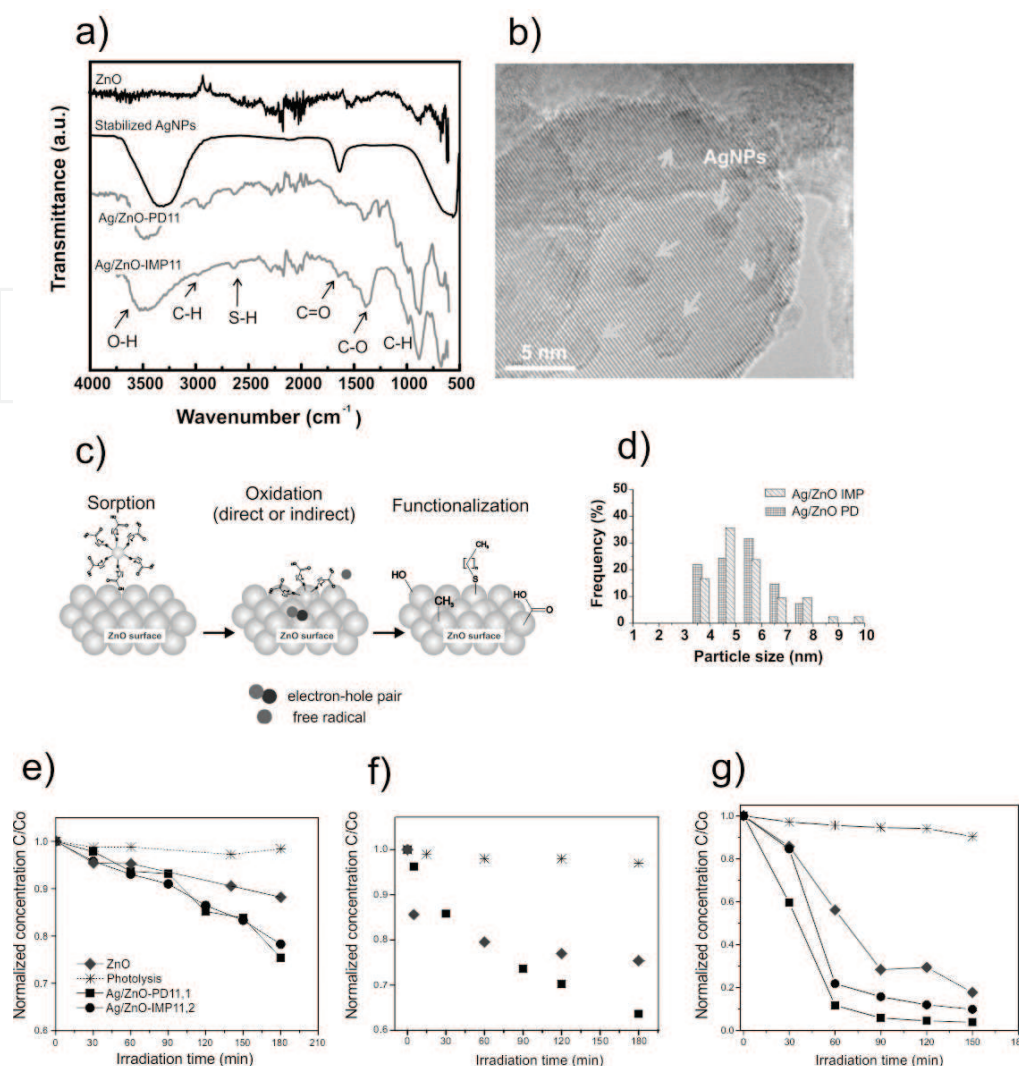**Figure 5.** Schematic illustration of the photocatalytic process in the ZnO/GO hybrid semiconductor.

**Figure 6.** FTIR (a) and TEM image (b) of the as-synthesized photocatalyst functionalized ZnO by silver nanoparticles. Schematic illustration of the functionalization by PD method. (c). Histogram of silver particle size (d). Photocatalytic degradation of bisphenol A (e), triclosan (f), and RhB (g).

photocatalyst surface with S-H, C-O, and hydroxyl groups ($^{-}$OH) creates defect sites advantageous in photocatalysis. Silver-experienced redox processes during PD functionalization, for instance, oxidation ($Ag^{+}/Ag^{0}$, +0.799 eV vs. SHE) by photogenerated holes (+2.75 eV, vs. SHE) and free radicals. They reduce again into the zero-valence form ($Ag^{0}$) by photoexcited electrons. This method favors insertion of ionic silver $Ag^{+}$ into ZnO crystalline structure perceived as an expansion of lattice parameters measured by XRD. The new attached silver possibly anchors on the surface defect sites of ZnO [25, 26]. The role of the metallic modifier in Ag/ZnO is to promote the pair electron-hole ($e^{-}/h^{+}$) separation and to increase the photocatalyst sensitivity toward visible light, in our case, evidenced as an absorption in the visible region by UV-Vis spectroscopy.

The IMP functionalization mechanism is different in the sense that silver nanoparticles and ZnO interaction is a function of the reaction time for an optimum of 2 h. For instance, the sample 1%Ag/ZnO-IMP11,2 synthesized using 1 wt.% Ag at pH 11 and 2 h under vigorous

stirring results in heterogeneously distributed silver nanoparticles of average size of 15 nm determined by Scherrer equation. The surfactant decomposes almost completely during the heating (at 300°C) that releases AgNPs onto ZnO surface. As before, residuals S-H and C-H functionalizing the ZnO surface was observed by IR (**Figure 6a**). Similarly, the as-synthesized 1%Ag/ZnO-IMP samples absorb in visible region of the spectrum and silver nanoparticles induce a surface-localized plasmon resonance.

It is challenging to control the metallic particle size because the nanoparticles have the trend to form agglomerates. The deposition of silver nanoparticles over metallic oxides from pre-formed nanoparticles using, for example, chemical vapor deposition [27] has been used, but IMP and PD methods demonstrate to be a successful bulk functionalization of ZnO at room temperature and atmospheric pressure. The increase of photocatalytic efficiency by silver-modified ZnO is demonstrated on the degradation of endocrine disruptors (i.e., bisphenol-A), an emergent contaminant (i.e., triclosan), and a dye (i.e., RhB) under visible light, which represents an important achievement in the use of solar-driven Ag/ZnO photocatalysts.

**Figure 6e-g** shows the progress of the contaminant photodegradation under visible light (365 nm, 0.97 mW/cm$^2$, 8 W 3UV-38 UVP Inc. lamp, lab-made reactor) at 20°C. The results show that 25% of bisphenol-A (10 mg/L) was destroyed after 3 h using Ag/ZnO-PD, and it represents an improvement of 100% compared with ZnO. A total of 35% of initial triclosan (20 mg/L) was destroyed within 3 h using Ag/ZnO-IMP11, represents an improvement of 45% compared with ZnO. Finally, 90% of dye discoloration is obtained with Ag/ZnO-PD11, being only 20% better than ZnO.

Similarly, the photocatalysts were tested under UV light (302 nm). The use of BET surface area normalization of the apparent rate constant (k$_{app}$/BET ssa) in photocatalysis was proposed to clearly demonstrate that ZnO nanoagglomerates is 400% faster than Pi-25, a TiO$_2$ well-known and extensively used photocatalyst from Degussa. The bandgap energy of ZnO and titanium dioxide (TiO$_2$) is basically the same (3.2 eV). However, the valence and conduction bands exhibit differences in electric potential values; whose reported values are in the range of −0.45 to 2.75 eV vs. NHE and − 0.1 to 3.1 eV vs. NHE, for ZnO and TiO$_2$, respectively [28, 29]. Thus, the photogenerated holes in ZnO have strong enough oxidizing power to decompose most organic compounds. Furthermore, 1%Ag/ZnO-PD11,1 photocatalytic activity is 370% faster than ZnO attributed to the photoexcited electron trapping in the metallic primary (e$^-$/h$^+$ pair) and secondary active species (free radicals, i.e., $^\bullet$OH) for the oxidation of bisphenol-A. The effect of pH, photocatalyst dosage, and bisphenol-A concentration on the kinetic rate constant were also studied extensively and reported [3].

### 2.3. ZnO immobilization by organic molecules: poly (acrylic acid)

The utilization of powder photocatalyst may end unpractical for industrial scales because of the technical challenges like efficient dispersion and finally difficult separation of photocatalyst after the reaction that may entail important energetic costs and sometimes even producing a secondary pollution. Besides, photocorrosion is an important drawback in photocatalysis, and the anchoring of silver has been proved to control its progress. The

immobilization of ZnO into organics tends to solve both the difficulty of photocatalyst dispersion and recuperation for a cyclic usage together with an improvement of the photostability [30]. The organics that have been reported for immobilization of TiO$_2$ comprise polyaniline [31, 32] and polypyrrole [33] that are hydrophobic and opaque, then it is incompatible for aqueous applications. Hydrogels, based on acrylic polymers, allow effective transport of water and other dissolved molecules due to their hydrophilicity and high swelling capacity. This kind of polymers shows stimuli-responsive properties to pH, temperature, solvent composition, and ionic strengths. Hydrogels come to be an ideal choice for Ag/ZnO photocatalyst immobilization since they are colorless and visually transparent, which permits penetration of light (**Figure 7e**).
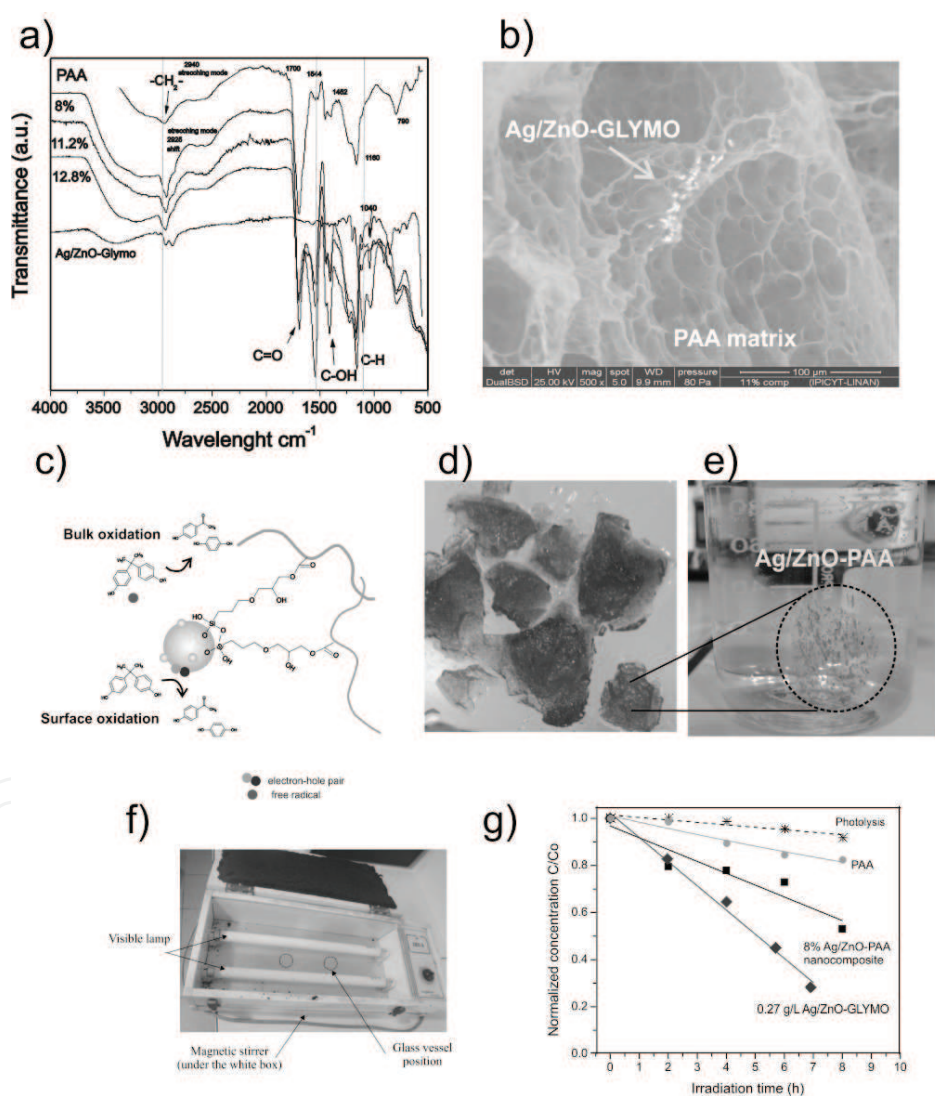


**Figure 7.** FTIR (a) and E-SEM image (b) of the as-synthesized Ag/ZnO-PAA. Schematic representation of the ligands between photocatalyst pending from the PAA chain and its photocatalytic role (c). Semi-swell Ag/ZnO-PAA composite (d) and reaction vessel containing photocatalyst dissolved in the pollutant solution (e).Home made photocatalytic reactor operated at room temperature and pressure (f). Photocatalytic degradation of bisphenol-A (g).

The general mechanism for the immobilization of Ag/ZnO into a poly (acrylic acid) (PAA) matrix involves the use of GLYMO as photocatalyst stabilizer and coupling agent. Infrared analysis (FTIR) shows characteristic bands at 916 and 1260 $cm^{-1}$ for free epoxide functional groups, in pure GLYMO and Ag/ZnO-GLYMO, meaning that epoxide do not react with Ag/ZnO surface, as desired. Disappearance of bands at 823 and 780 $cm^{-1}$, corresponding to C-H from the methoxysilyl groups ($CH_3O^-$) of GLYMO, indicates two processes: hydrolysis of methoxy group and reaction with Ag/ZnO surface by weak bond such as hydrogen bonds. In addition, the peak at 1030 $cm^{-1}$ corresponds to the formation of self-assembled monolayer Si-O-Si on Ag/ZnO surface, and confirms the efficient silanization of the photocatalyst (**Figure 7a**). Lastly, the interaction between the free tail of Ag/ZnO-GLYMO (highly reactive epoxy groups) and the carboxylic groups of PAA gives strong interaction and immobilization into the polymeric matrix.

Two possible arrangements of the photocatalyst bonded to the polymer matrix are proposed: (i) a photocatalyst pending from the PAA chain (**Figure 7c**) and (ii) a cross-linked–like structure, where the photocatalyst is the bridge between two PAA chains.

Environmental SEM chamber allow us for first time to obtain images of 3D network of cross-linked PAA under low vacuum that gives us a time-window of approximately 30 minutes for the analysis before dehydration (**Figure 7b**). SEM-EDX confirms the homogeneous dispersion of photocatalyst within the PAA matrix on 8%Ag/ZnO-PAA composites. The swelling capacity of the composite increases with photocatalyst content (5–13 wt.%) due to the high hydrophilicity of Ag/ZnO (**Figure 7d**). In addition, the composite photostability after 16 h of UV (365 nm) exposure was corroborated by FTIR and TGA analysis.

This enhanced photochemical stability has the potential of use as resistant composite packing material for continuous treatment of water under UV irradiation. This last aspect was first tested in batch experiments toward the degradation of bisphenol-A. Thus, **Figure 7g** shows the time evolution of the bisphenol-A photodegradation under visible light (>450 nm, 8 uW/cm$^2$, 8 W Hampton Bay lamp, home-made reactor in **Figure 7f**) at 50°C. On the other hand, 47% of the initial concentration of 10 mg/L is degraded within 7 h by 8%Ag/ZnO-PAA composite, it represents a decrease of 50% compared with Ag/ZnO-GLYMO. The composite was reused in a second consecutive cycle without washing that results in an improvement of 40% compared with the first cycle. It is necessary to highlight that the sorption of bisphenol-A in dark conditions was not important; therefore, regeneration of the composite is not necessary in continuous water treatments. Ag/ZnO-PAA composites like those synthesized in this study are less sensitive to saturation compared to zeolites and carbon materials.

# 3. Bismuth oxychloride (BiOCl)

Bismuth oxyhalides BiOCl (X:Cl, Br, and I) are a new class of semiconductors that have recently attracted attentions in the photocatalytic process due to their relatively slow electron-hole recombination process. BiOXs are conformed by $Bi^{3+}$, $O^{2-}$, and halide ($X^-$) ions stacked in [X-Bi-O-Bi-X]$_n$ layers, giving a tetragonal structure with no linkers interactions with halide
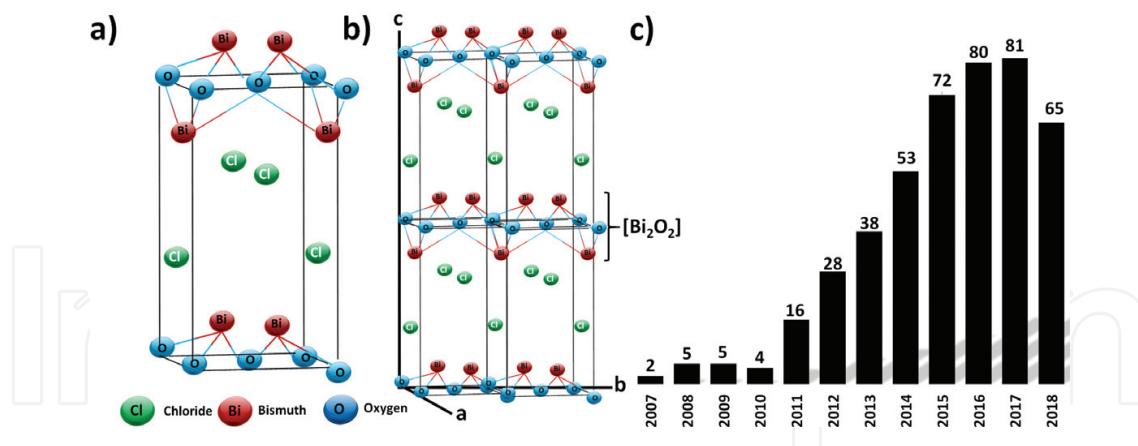
**Figure 8.** Scheme of unit cell (a), crystal structure BiOCl with {001} facet (b) and growing of articles of BiOCl in the photocatalytic process in later years (c).

along the C axis as showed in **Figure 8a**, **b**. The photocatalytic activity is due to $[Bi_2O_2]$ layers intercalated of double halogen atoms that allow a better separation of the electron-hole pairs. The bismuth oxychloride (BiOCl) is a solid inorganic compound, not toxic, of pearlescent white color and due its brightness has been used in the cosmetic industry. There is a record not greater than 500 articles reported in the Scopus database concerning the use of BiOCl, as photocatalyst; this review was realized in June 2018 (**Figure 8c**) and the first publications appeared in 2007 with a growing interest during the last years.

The BiOCl has a bandgap of 3.2–3.5 eV and the valence band is constituted of $O_{2p}$ and $Cl_{3p}$; while the conduction band has $Bi_{6p}$ according to density functional theory (DFT), whereby when excited, the electrons from Cl atoms are displaced at bismuth orbital [34].

Most studies of BiOCl photocatalyst are focused on enhancing the photocatalytic activity for environmental remediation, especially for dyes degradation during water treatment. Due to the bandgap, its photocatalytic activity, under UV irradiation, has shown a similar or better photocatalytic activity than $TiO_2$ [35]. Some "model" dyes used to evaluate the photocatalytic activity with BiOCl are methylene blue, methyl orange [36], and Rh B [37]. In spite of the bandgap of BiOCl, there are reports wherein demonstrate an excellent degradation of RhB under visible light [38].

However, some challenges remain for BiOCl as most photocatalysts also face; one challenge is its activation under visible light due to the limited absorption of such radiation. A variety of strategies have been employed to get better light absorption and to decrease the charge carrier recombination, such as the heterojunction, doping impurity, and metallization of the surface. Modifications consider the presence of metal elements or compounds like Ag [39, 40], AgCl [41], Fe [42], and Bi [43], also with materials carbon-based as graphene [44], graphene oxide [45], and with other semiconductors as $Co_3O_4$ [46], BiOI [47], and $TiO_2$ [48–50]. However, most researches evaluated the photocatalytic activity for degradation of dyes, considering the RhB in many cases. Other pollutant photodegradation studies are bisphenol A using Fe-BiOCl under visible light [42], sulfanilamide with BiOCl-RGO [51], and phenol under visible light with BiOCl-TiO₂ composite [50]. Nowadays, the BiOCl is being investigated to reduce of carbon dioxide ($CO_2$) [52].

### 3.1. Experimental section for BiOCl

The photocatalytic activity was evaluated using two commercial BiOCl samples, which were modified with silver (Ag), graphene oxide (OG), and $TiO_2$. The BiOCl samples were named as P2600 and SB. The P2600 sample is a hydrophobic sample while SB sample is hydrophilic sample.

#### 3.1.1. Modification of BiOCl samples

The modification of BiOCl with Ag and OG was carried out by photodeposition method, which consisted in disperse 500 mg of BiOCl (P2600 and SB) in deionized water during 30 minutes, then the particles of the Ag or OG were added in different percentages; in the case of Ag were 2.0, 0.5, and 0.1% w/w and for OG were 0.5 and 0.1% w/w. Then, the sample was irradiated using a Q200 reactor ($\lambda$ = 250 nm, 304 mW/cm$^2$) for 3 h with continuous stirring. Later, the samples were centrifuged and thoroughly water washed for several cycles, and finally, they were dried at 70°C for 24 h. The composites with $TiO_2$ were prepared by solvothermal method with different weight percentages of $TiO_2$ (25, 50, and 75% w/w).

#### 3.1.2. Characterization

The crystal structure of the synthesized photocatalysts was analyzed by X-ray diffraction (XRD) using a DX8 advance diffractometer (Bruker) with: Cu K$\alpha$ radiation, 35 kV, 25 mA, $\lambda$ = 0.15418 nm over the 2$\theta$ range of 10–80° in a step of 0.02°s$^{-1}$. The analysis of surface morphology and microstructure of the samples was carried out by a QUANTA 200 environmental scanning electron microscope.

#### 3.1.3. Photocatalytic activity

The photocatalytic activity was evaluated with two pollutants. The samples modified with Ag and OG were evaluated for RhB degradation under visible light, the RhB degradation was followed by UV-Vis spectrophotometer at 552 nm. The composites with $TiO_2$ were evaluated for Phenol degradation under visible light (Xenon lamp; Oriel 300 W; $\lambda$ = 450 nm). Monitoring of phenol degradation was carried out by high performance liquid chromatography (HPLC) using a C18 column with a mobile phase of acetonitrile-water (27–75%) with a flow of 0.5 mL min$^{-1}$.

### 3.2. Results and discussion

Both pure BiOCl samples (P2600 and SB) showed overlapping flakes forming flower-like morphology, the size of flakes were of 10–60 microns approximately in P2600 samples (**Figure 9a**), while SB samples displayed a size of flakes about 9–34 microns (**Figure 9b**).

In the Ag-modified samples, small BiOCl-impregnated particles on the flakes were observed, in the case of the modified SB samples, a major impregnation of Ag particles was noticed (**Figure 9c**) in comparison with Ag-P2600 sample (**Figure 9d**); probably due to hydrophobic character of P2600 sample avoiding that Ag particles could have contact with the photocatalyst. Regarding OG-BiOCl samples, in both modified photocatalysts, it was observed
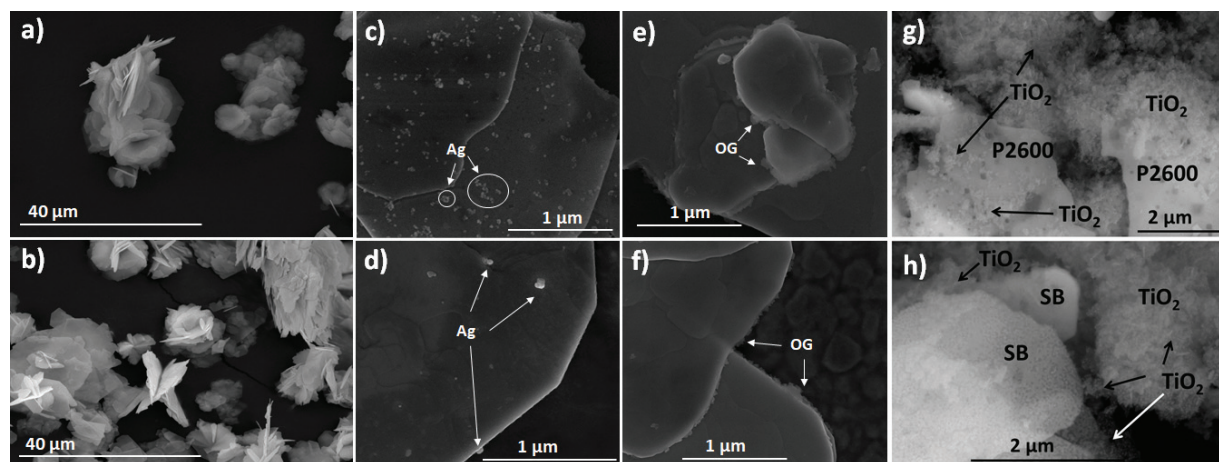
**Figure 9.** SEM images of BiOCl pure samples; SB (b) and P2600 (a). BiOCl modified with silver; Ag-SB (c) and Ag-P2600 (d). BiOCl modified with graphene oxide; OG-SB (e) and OG-P2600 (f). BiOCl modified with titanium dioxide; TiO$_2$-SB (g) and TiO$_2$-P2600 (h).

that small sheet of OG was deposited in the flakes of BiOCl, mainly in the edges of flakes as it is observed in **Figure 9e-f**. While in the composites of TiO$_2$-BiOCl, the generated TiO$_2$ was incrusted as small agglomerated particles on the BiOCl flakes (**Figure 9c-d**). Both photocatalysts could promote a better separation of photocharges generated during the reaction and therefore a better photocatalytic activity (**Figure 9g-h**).

The RhB degradation under visible light with Ag-BiOCl is shown in **Figure 10a**, **b**, the maximum degradation of RhB was obtained with pure BiOCl; and 30 and 40% of RhB degradation with P2600 and SB were obtained, respectively. In the case of Ag-SB, as the percentage of Ag increased, the photocatalytic activity decreased, while with Ag-P2600 was observed a greater degradation with 0.5% Ag than with 0.1%Ag. The presence of Ag in the BiOCl generates a decrease of photocatalytic activity, this result may be due to the presence of Ag in two oxidation states (Ag$^0$ and Ag$^{1+}$) observed in the XRD specter (**Figure 10c**, **d**), which may be acting as recombination sites. The modification with Ag incites a displacement of the [001] peak in the XRD specter probably due to the change of atoms of Bi by atoms of Ag because both elements have a similar ionic radius. Likewise, change of intensity in the [002] and [101] peaks in the spectra may be associated with a modification of the crystalline phase. This change in the Ag-BiOCl may affect the photocatalytic activity.

With the OG-BiOCl sample, the photocatalytic activity was different, since with low percentage of OG, the photocatalytic activity increased. The OG-SB sample (0.1% of OG) gave the greater degradation of RhB, while the OG-P2600 (0.1% of OG) and pure P2600 had the same degradation percentage (**Figure 11a**, **b**). In the XRD spectra of OG-BiOCl was observed, a decrement in intensities of [001], [102], and [112] peaks, and an intensity increment for [002] peak as the OG percentage increased. This result indicates that OG induces a better orientation of {001} facet in both BiOCls (**Figure 11c**, **d**).

Referring to TiO$_2$-BiOCl composite, its photocatalytic activity was evaluated for phenol degradation under visible light. The better composites were TiO$_2$-P2600 (75–25%) giving 45% of
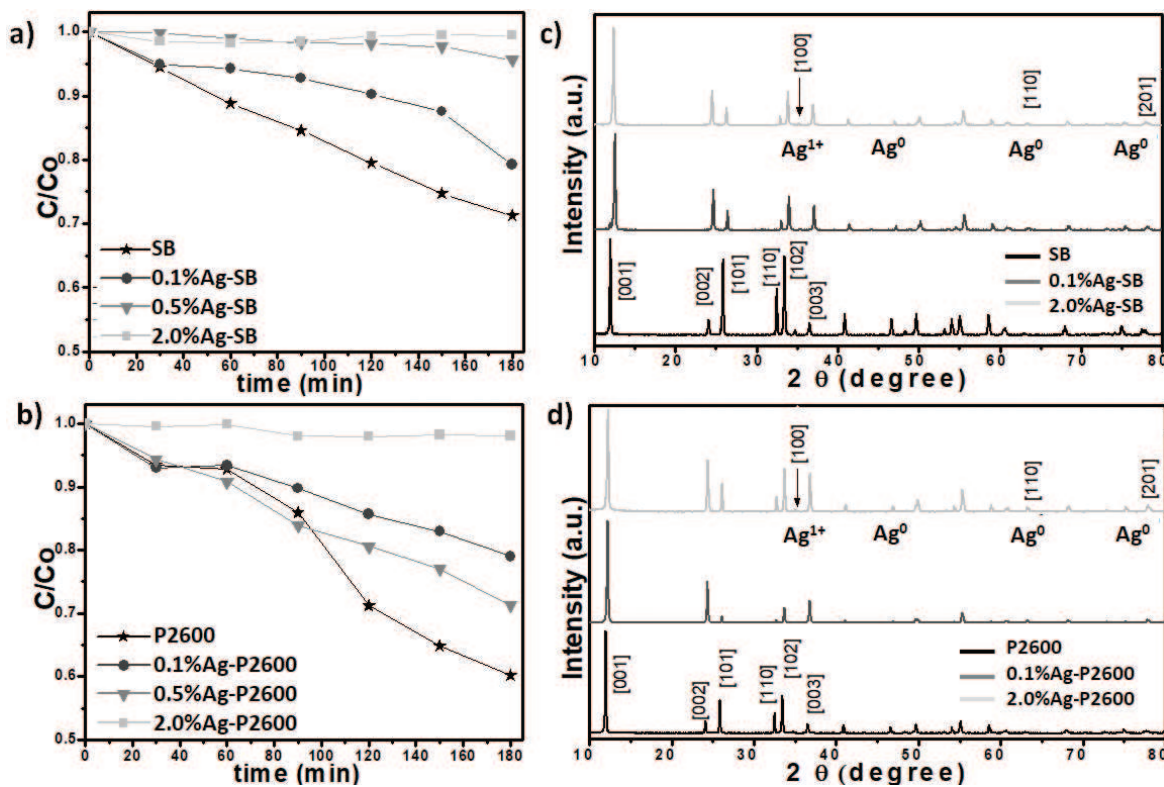
**Figure 10.** RhB degradation under visible irradiation with BiOCl pure and modified with silver; Ag-SB (a) and Ag-P2600 (b). XRD spectra of BiOCl samples; Ag-SB (c) and Ag-P2600 (d).

phenol degradation and TiO$_2$-SB (50–50%) giving 36% of phenol degradation during 6 h of reaction (**Figure 12a**, **b**). For the composite TiO$_2$-P2600 conforming the percentage of TiO$_2$ decreased, the photocatalytic activity also decreased. Such results confirm that there is a good interaction between both photocatalysts (BiOCl and TiO$_2$), in the TiO$_2$-P2600 composites, the size and hydrophobicity of P2600 played an important role in the adsorption of phenol on the surface, and therefore, gave a higher photocatalytic activity. In addition, higher TiO$_2$ percentage generated the appropriate heterojunction. In the XRD spectrum of TiO$_2$-BiOCl, the presence of peaks from both photocatalysts was observed (**Figure 12c, d**), also an overlap of the peaks [002] and [101] of BiOCl with the peak of [001] of TiO$_2$. In TiO$_2$-SB composites, it observed a lower intensity for [001] peak corresponding to BiOCl. Regarding TiO$_2$-SB composites, the SB exhibited a smaller size and hydrophilic character; then it was necessary that less amount of TiO$_2$ is active under visible light, and an increment of TiO$_2$ could generate the recombination of electron-hole pairs decreasing the photocatalytic activity.

The results obtained in our study offer a promising direction for the design of more practical and efficient photocatalysts to be used under visible light. In addition, the photocatalysis using BiOCl is becoming a promising research topic due to its fascinating characteristics, and it is necessary to study and understand the synthesis methods, morphology, predominant facets that improve the photocatalytic activity in all visible irradiations in order to achieve the mineralization of pollutants. Currently, our research group is working with the generation of biofuels by photocatalysis using BiOCl.
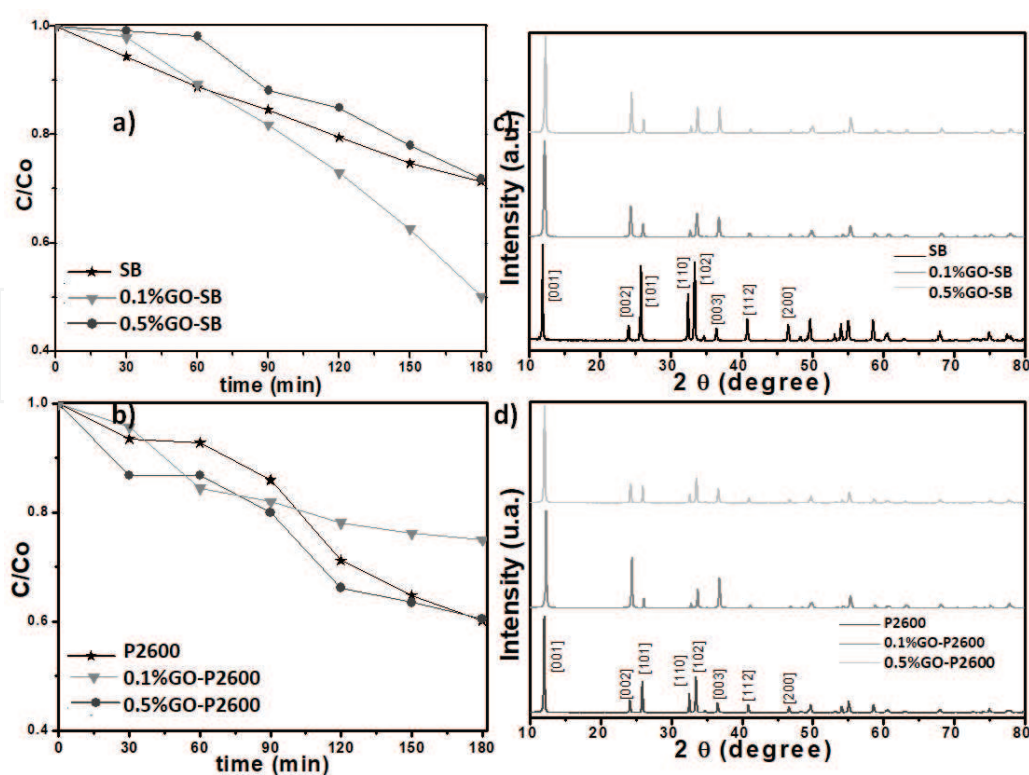
**Figure 11.** RhB degradation under visible irradiation with BiOCl pure and modified with graphene oxide; OG-SB (a) and OG-P2600 (b). XRD spectra of BiOCl samples; OG-SB (c) and OG-P2600 (d).
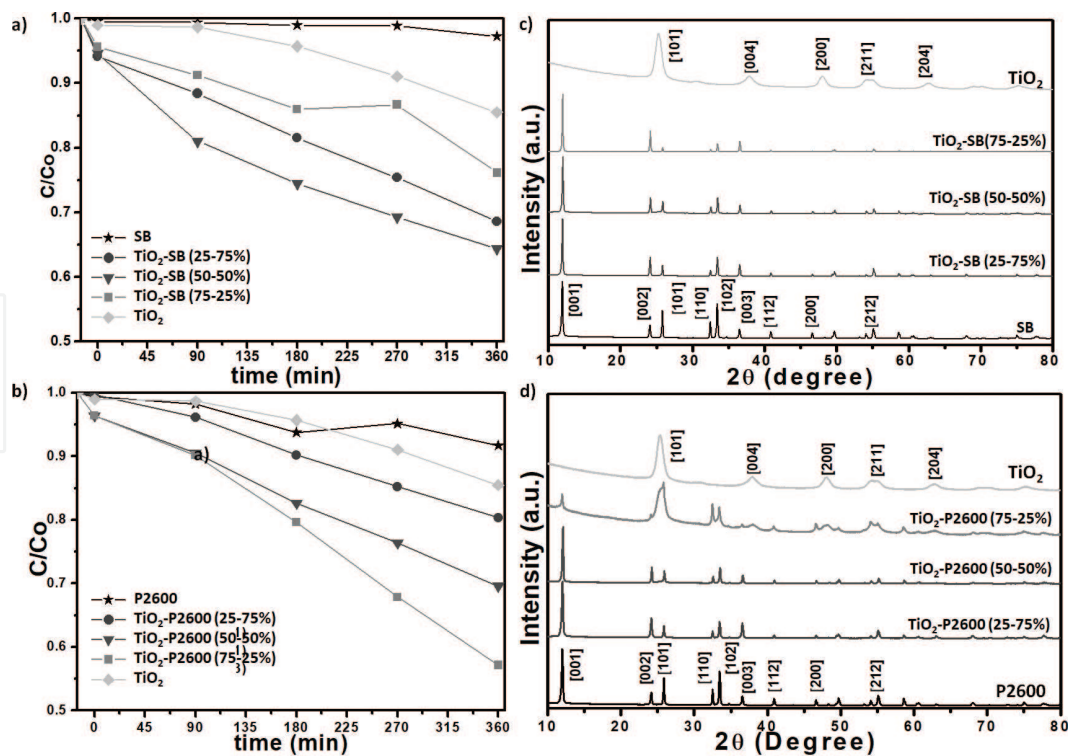


**Figure 12.** Phenol degradation under visible irradiation with BiOCl pure and modified with titanium dioxide; TiO$_2$-SB (a) and TiO$_2$-P2600 (b). XRD spectra of BiOCl samples; TiO$_2$-SB (c) and TiO$_2$-P2600 (d).

## Author details

Vladimir A. Escobar Barrios[1]*, Dalia Verónica Sánchez Rodríguez[1],
Nancy Ayerim Cervantes Rincón[2] and Alma Berenice Jasso-Salcedo[3]

*Address all correspondence to: vladimir.escobar@ipicyt.edu.mx

1 Instituto Potosino de Investigación Científica y Tecnólogica, A.C. (IPICYT), Advanced
Materials Division, San Luis Potosí, México

2 Instituto Potosino de Investigación Científica y Tecnólogica, A.C. (IPICYT), Environmental
Sciences Division, San Luis Potosí, México

3 Department of Materials and Environmental Chemistry, Stockholm University, Stockholm,
Sweden

## References

[1] Lacombe S, Keller N. Photocatalysis: Fundamentals and applications in JEP 2011. Environmental Science and Pollution Research. 2012;**19**:3651-3654. DOI: 10.1007/s11356-012-1040-8

[2] Wang ZL, Kong XY, Ding Y, Gao P, Hughes WL, Yang R, et al. Semiconducting and piezoelectric oxide nanostructures induced by polar surfaces. Advanced Functional Materials. 2004;**14**:943-956. DOI: 10.1002/adfm.200400180

[3] Jasso-Salcedo AB, Hoppe S, Pla F, Escobar-Barrios VA, Camargo M, Meimaroglou D. Modeling and optimization of a photocatalytic process: Degradation of endocrine disruptor compounds by Ag/ZnO. Chemical Engineering Research and Design. 2017;**128**:174-191

[4] Man MT, Kim JH, Jeong MS, Do ATT, Lee HS. Oriented ZnO nanostructures and their application in photocatalysis. Journal of Luminescence. 2017;**185**:17-22. DOI: 10.1016/j.jlumin.2016.12.046

[5] Cantwell G, Harsch WC, Jogai B. Valence-band ordering in ZnO. Physical Review B: Condensed Matter and Materials Physics. 1999;**60**:2340-2344. DOI: 10.1103/PhysRevB.60.2340

[6] Porter F. Modified Metallic Oxides for Efficient Photocatalysis. First edit; 1991

[7] Jia W, Shang Y, Gong L, Chen X. Synthesis of Al-ZnO nanocomposite and its potential application in photocatalysis and electrochemistry. Inorganic Chemistry Communications. 2018;**88**:51-55. DOI: 10.1016/j.inoche.2017.12.013

[8] Schmidt-Mende L, MacManus-Driscoll JL. ZnO–Nanostructures, defects, and devices. Materials Today. 2007;**10**:40-48. DOI: 10.1016/S1369-7021(07)70078-0

[9] Daneshvar N, Aber S, Seyed Dorraji MS, Khataee AR, Rasoulifard MH. Photocatalytic degradation of the insecticide diazinon in the presence of prepared nanocrystalline ZnO

powders under irradiation of UV-C light. Separation and Purification Technology. 2007;**58**:91-98. DOI: 10.1016/j.seppur.2007.07.016

[10]  Wang C, Astruc D. Recent developments of metallic nanoparticle-graphene nanocatalysts. Progress in Materials Science. 2018;**94**:306-383. DOI: 10.1016/j.pmatsci.2018.01.003

[11]  Bai X, Wang L, Zhu Y. Visible photocatalytic activity enhancement of $ZnWO_4$ by graphene hybridization. ACS Catalysis. 2012;**2**:2769-2778. DOI: 10.1021/cs3005852

[12]  Shen Y, Fang Q, Chen B. Environmental applications of three-dimensional graphene-based macrostructures: Adsorption, transformation, and detection. Environmental Science & Technology. 2015;**49**:67-84. DOI: 10.1021/es504421y

[13]  McClellan K, Halden RU. Pharmaceuticals and personal care products in archived U.S. biosolids from the 2001 EPA national sewage sludge survey. Water Research. 2010;**44**: 658-668. DOI: 10.1016/j.watres.2009.12.032

[14]  Walters E, McClellan K, Halden RU. Occurrence and loss over three years of 72 pharmaceuticals and personal care products from biosolids-soil mixtures in outdoor mesocosms. Water Research. 2010;**44**:6011-6020. DOI: 10.1016/j.watres.2010.07.051

[15]  Jasso-Salcedo AB, Palestino G, Escobar-Barrios VA. Effect of Ag, pH, and time on the preparation of Ag-functionalized zinc oxide nanoagglomerates as photocatalysts. Journal of Catalysis. 2014;**318**:170-178

[16]  Kislov N, Lahiri J, Verma H, Goswami DY, Stefanakos E, Batzill M. Photocatalytic degradation of methyl orange over single crystalline ZnO: Orientation dependence of photoactivity and photostability of ZnO. 2009;**25**:3310-3315. DOI: 10.1021/la803845f

[17]  Santiago-Morales J, Gómez MJ, Herrera-López S, Fernández-Alba AR, García-Calvo E, Rosal R. Energy efficiency for the removal of non-polar pollutants during ultraviolet irradiation, visible light photocatalysis and ozonation of a wastewater effluent. Water Research. 2013;**47**:5546-5556. DOI: 10.1016/j.watres.2013.06.030

[18]  Xu F, Chen J, Kalytchuk S, Chu L, Shao Y, Kong D, et al. Supported gold clusters as effective and reusable photocatalysts for the abatement of endocrine-disrupting chemicals under visible light. Journal of Catalysis. 2017;**354**:1-12. DOI: 10.1016/j.jcat.2017.07.027

[19]  Dai Y, Yin L. Synthesis and photocatalytic activity of Ag-Ti-Si ternary modified-$Bi_2O_3$ nanoporous spheres. Materials Letters. 2015;**142**:225-228. DOI: 10.1016/j.matlet.2014.12.013

[20]  Niu J, Dai Y, Yin L, Shang J, Crittenden JC. Photocatalytic reduction of triclosan on Au–$Cu_2O$ nanowire arrays as plasmonic photocatalysts under visible light irradiation. Physical Chemistry Chemical Physics. 2015;**17**:17421-17428. DOI: 10.1039/C5CP02244D

[21]  Zhao L, Deng J, Sun P, Liu J, Ji Y, Nakada N, et al. Nanomaterials for treating emerging contaminants in water by adsorption and photocatalysis: Systematic review and bibliometric analysis. Science of the Total Environment. 2018;**627**:1253-1263. DOI: 10.1016/j.scitotenv.2018.02.006

[22] Chen F, An W, Liu L, Liang Y, Cui W. Highly efficient removal of bisphenol A by a three-dimensional graphene hydrogel-AgBr@rGO exhibiting adsorption/photocatalysis synergy. Applied Catalysis B: Environmental. 2017;**217**:65-80. DOI: 10.1016/j.apcatb.2017.05.078

[23] Fu H, Xu T, Zhu S, Zhu Y. Photocorrosion inhibition and enhancement of photocatalytic activity for ZnO via hybridization with $C_{60}$. Environmental Science & Technology. 2008; **42**:8064-8069. DOI: 10.1021/es801484x

[24] Xu T, Zhang L, Cheng H, Zhu Y. Significantly enhanced photocatalytic performance of ZnO via graphene hybridization and the mechanism study. Applied Catalysis B: Environmental. 2011;**101**:382-387. DOI: 10.1016/j.apcatb.2010.10.007

[25] Xie W, Li Y, Sun W, Huang J, Xie H, Zhao X. Surface modification of ZnO with Ag improves its photocatalytic efficiency and photostability. Journal of Photochemistry and Photobiology A: Chemistry. 2010;**216**:149-155. DOI: http://dx.doi.org/10.1016/j.jphotochem.2010.06.032

[26] Kawano K, Komatsu M, Yajima Y, Haneda H, Maki H, Yamamoto T. Photoreduction of Ag ion on ZnO single crystal. Applied Surface Science. 2002;**189**:265-270

[27] Salaün A, Hamilton JA, Iacopino D, Newcomb SB, Nolan MG, Padmanabhan SC, et al. The incorporation of preformed metal nanoparticles in zinc oxide thin films using aerosol assisted chemical vapour deposition. Thin Solid Films. 2010;**518**:6921-6926

[28] Li B, Cao H. ZnO@graphene composite with enhanced performance for the removal of dye from water. Journal of Materials Chemistry. 2011;**21**:3346-3349. DOI: 10.1039/c0jm03253k

[29] Xiong Z, Zhang LL, Ma J, Zhao XS. Photocatalytic degradation of dyes over graphene-gold nanocomposites under visible light irradiation. Chemical Communications. 2010;**46**: 6099-6101. DOI: 10.1039/c0cc01259a

[30] Jasso-Salcedo AB, Meimaroglou D, Hoppe S, Pla F, Escobar-Barrios VA. Surface modification and immobilization in poly (acrylic acid) of Ag/ZnO for photocatalytic degradation of endocrine-disrupting compounds. Journal of Applied Polymer Science. 2016;**133**:1-12

[31] Leng C, Wei J, Liu Z, Xiong R, Pan C, Shi J. Facile synthesis of PANI-modified $CoFe_2O_4$-$TiO_2$ hierarchical flower-like nanoarchitectures with high photocatalytic activity. Journal of Nanoparticle Research. 2013;**15**:1643

[32] Zhang H, Zong R, Zhu Y. Photocorrosion inhibition and photoactivity enhancement for zinc oxide via hybridization with monolayer polyaniline. Journal of Physical Chemistry C. 2009;**113**:4605-4611

[33] Lu B, Liu M, Shi H, Huang X, Zhao G. A novel photoelectrochemical sensor for bisphenol A with high sensitivity and selectivity based on surface molecularly imprinted polypyrrole modified $TiO_2$ nanotubes. Electroanalysis. 2013;**25**:771-779

[34] Yang W, Wen Y, Chen R, Zeng D, Shan B. Study of structural, electronic and optical properties of tungsten doped bismuth oxychloride by DFT calculations. Physical Chemistry Chemical Physics. 2014;**16**:21349-21355. DOI: 10.1039/C4CP02801E

[35] Sun D, Li J, Feng Z, He L, Zhao B, Wang T, et al. Solvothermal synthesis of BiOCl flower-like hierarchical structures with high photocatalytic activity. Catalysis Communications. 2014;**51**:1-4. DOI: 10.1016/j.catcom.2014.03.004

[36] Sarwan B, Pare B, Acharya AD. The effect of oxygen vacancies on the photocatalytic activity of BiOCl nanocrystals prepared by hydrolysis and UV light irradiation. Materials Science in Semiconductor Processing. 2014;**25**:89-97. DOI: 10.1016/j.mssp.2013.09.015

[37] Hao HY, Xu YY, Liu P, Zhang GY. BiOCl nanostructures with different morphologies: Tunable synthesis and visible-light-driven photocatalytic properties. Chinese Chemical Letters. 2015;**26**:133-136. DOI: 10.1016/j.cclet.2014.11.022

[38] Wang Q, Hui J, Huang Y, Ding Y, Cai Y, Yin S, et al. The preparation of BiOCl photocatalyst and its performance of photodegradation on dyes. Materials Science in Semiconductor Processing. 2014;**17**:87-93. DOI: 10.1016/j.mssp.2013.08.018

[39] Gao Y, Wang L, Li Z, Li C, Cao X, Zhou A, et al. Microwave-assisted synthesis of flower-like Ag-BiOCl nanocomposite with enhanced visible-light photocatalytic activity. Materials Letters. 2014;**136**:295-297. DOI: 10.1016/j.matlet.2014.08.026

[40] Zhang Z, Zhou Y, Yu S, Chen M, Wang F. Ag-BiOCl nanocomposites prepared by the oxygen vacancy induced photodeposition method with improved visible light photocatalytic activity. Materials Letters. 2015;**150**:97-100. DOI: 10.1016/j.matlet.2015.03.011

[41] Cheng J, Wang C, Cui Y, Sun Y, Zuo Y, Wang T. Large improvement of visible-light-driven photocatalytic property in AgCl nanoparticles modified black BiOCl microsphere. Materials Letters. 2014;**127**:28-31. DOI: 10.1016/j.matlet.2014.04.012

[42] Xia J, Xu L, Zhang J, Yin S, Li H, Xu H, et al. Improved visible light photocatalytic properties of Fe/BiOCl microspheres synthesized via self-doped reactable ionic liquids. CrystEngComm. 2013;**15**:10132. DOI: 10.1039/c3ce41555d

[43] Hu J, Xu G, Wang J, Lv J, Zhang X, Zheng Z, et al. Photocatalytic properties of Bi/BiOCl heterojunctions synthesized using an in situ reduction method. New Journal of Chemistry. 2014;**38**:4913-4921. DOI: 10.1039/C4NJ00794H

[44] Gao F, Zeng D, Huang Q, Tian S, Xie C. Chemically bonded graphene/BiOCl nanocomposites as high-performance photocatalysts. Physical Chemistry Chemical Physics. 2012;**14**:10572. DOI: 10.1039/c2cp41045a

[45] Kang S, Pawar RC, Pyo Y, Khare V, Lee CS. Size-controlled BiOCl–RGO composites having enhanced photodegradative properties. Journal of Experimental Nanoscience. 2016;**11**:259-275. DOI: 10.1080/17458080.2015.1047420

[46] Tan C, Zhu G, Hojamberdiev M, Okada K, Liang J, Luo X, et al. $Co_3O_4$ nanoparticles-loaded BiOCl nanoplates with the dominant {001} facets: Efficient photodegradation of organic dyes under visible light. Applied Catalysis B: Environmental. 2014;**152–153**: 425-436. DOI: 10.1016/j.apcatb.2014.01.044

[47] Sun L, Xiang L, Zhao X, Jia CJ, Yang J, Jin Z, et al. Enhanced visible-light photocatalytic activity of BiOI/BiOCl heterojunctions: Key role of crystal facet combination. ACS Catalysis. 2015;**5**:3540-3551. DOI: 10.1021/cs501631n

[48] Liu Z, Xu X, Fang J, Zhu X, Li B. Synergistic degradation of eosin y by photocatalysis and electrocatalysis in UV irradiated solution containing hybrid BiOCl/TiO$_2$ particles. Water, Air, and Soil Pollution. 2012;**223**:2783-2798. DOI: 10.1007/s11270-011-1066-4

[49] Li L, Zhang M, Liu Y, Zhang X. Hierarchical assembly of BiOCl nanosheets onto bicrystalline TiO$_2$ nanofiber: Enhanced photocatalytic activity based on photoinduced interfacial charge transfer. Journal of Colloid and Interface Science. 2014;**435**:26-33. DOI: 10.1016/j.jcis.2014.08.022

[50] Sánchez-Rodríguez D, Méndez Medrano MG, Remita H, Escobar-Barrios V. Photocatalytic properties of BiOCl-TiO$_2$ composites for phenol photodegradation. Journal of Environmental Chemical Engineering. 2018;**6**:1601-1612. DOI: 10.1016/j.jece.2018.01.061

[51] Dong S, Pi Y, Li Q, Hu L, Li Y, Han X, et al. Solar photocatalytic degradation of sulfanilamide by BiOCl/reduced graphene oxide nanocomposites: Mechanism and degradation pathways. Journal of Alloys and Compounds. 2016;**663**:1-9. DOI: 10.1016/j.jallcom.2015.12.027

[52] Zhang L, Wang W, Jiang D, Gao E, Sun S. Photoreduction of CO$_2$ on BiOCl nanoplates with the assistance of photoinduced oxygen vacancies. Nano Research. 2015;**8**:821-831. DOI: 10.1007/s12274-014-0564-2